Biomedicine & Pharmacotherapy 156 (2022) 113885

Contents lists available at ScienceDirect

Biomedicine & Pharmacotherapy

journal homepage: www.elsevier.com/locate/biopha

Gundelia tournefortii inhibits hepatocellular carcinoma progression by lowering gene expression of the cell cycle and hepatocyte proliferation in immunodeficient mice

Johnny Amer [a,*], Ahmad Salhab [b], Nidal Jaradat [c], Samer Abdallah [d], Hanood Aburas [e], Suhaib Hattab [f], Mustafa Ghanim [b], Malik Alqub [a]

[a] Department of Allied and Applied Medical Sciences, Division of anatomy biochemistry and genetics, Faculty of Medicine and Health Sciences, An-Najah National University, P.O. Box 7, Nablus, Palestine
[b] Department of Biomedical Sciences, Faculty of Medicine and Health Sciences, An-Najah National University, P.O. Box 7, Nablus, Palestine
[c] Department of Pharmacy, Faculty of Medicine and Health Sciences, An-Najah National University, P.O. Box 7, Nablus, Palestine
[d] Department Biology and Biotechnology, Faculty of Science, An-Najah National University, P.O. Box 7, Nablus, Palestine
[e] Department of Pathology, Faculty of Medicine and Health Sciences, An-Najah National University, P.O. Box 7, Nablus, Palestine
[f] Department of Biomedical Sciences, Physiology, Pharmacology & Toxicology Division, Faculty of Medicine and Health Sciences, An-Najah National University, P.O. Box 7, Nablus, Palestine

ARTICLE INFO

Keywords:
Gundelia tournefortii
Cell cycle
Antiproliferative
Apoptosis-inducer
Liver cancer

ABSTRACT

Gundelia (G.) tournefortii has antibacterial, anti-inflammatory, and hypolipemic effects. We evaluated the anti-cancer effect of *G. tournefortii* in an hepatocellular carcinoma (HCC) mouse model of an HCC cell line (Hep3B) injected into NOD.CB17-Prkdc-SCID/NCrHsD male mice. Tumorigenicity was assessed by tumor size, histology, serum α-fetoprotein (αFP), and glypican 3 (GPC3). HCC-related gene expression of the cell cycle (Cyclin-dependent kinase inhibitor 2A (CDNK2A)), proliferation (MKI67), and platelet-derived growth factor receptor α (PDGFA) were measured. HCC cell cycle alterations, apoptosis, and antioxidant markers in serum and liver following treatment with *G. tournefortii* were determined. Signaling pathways of liver p53 and phosphorylated PI3K, AKT, and mTOR were also evaluated. Results indicate a significant increase in tumor size in HCC animals associated with elevated αFP, GPC3, and MKI67. Tumor markers of p53 and phosphorylated AKT/PI3K/mTOR signaling pathway were diminished, with less proliferating cells and reduced PDGFRA gene expression following *G. tournefortii* infection. H&E staining showed a remarkable reduction in inflammatory lesions in HCC mice treated with *G. tournefortii*. This result was in line with a significant delay in the G2/M phase of HCC-primary hepatocytes by 1.39- to 2.4-fold and reduced HCC necrosis associated with inhibited CDNK2A gene expression. Antioxidant activity was significantly lower in the HCC mice than in the control group. Moreover, *G. tournefortii* inhibited the HCC formation of 3D MCTS spheroids. *G. tournefortii* treatment markedly restored antioxidant levels and displayed anticancer and antiproliferative effects and could be a promising cancer therapy.

1. Introduction

Recently, the interest in herbal supplements and functional food products has increased due to their nutritional and health benefits [1–3]. *Gundelia (G.) tournefortii* is commonly known as tumble thistle, tumbleweed, and a'kub in Arabic. This annual herbaceous plant belongs to the Asteraceae (Compositae) family, is native to the irano-turanian region, and may be found in the Mediterranean areas of the east. It grows in semi-desert or sandy plains in Palestine, Jordan, Syria, Iraq, Iran, Azerbaijan, Anatolia, Armenia, Turkey, and other areas [4–6]. *G. tournefortii* is a spiny thistle-like perennial plant about 60 cm in height, its stems branch from the base, and it is almost hairless. Its leaves are leathery, rigid, and alternating with prominent yellow, red, or purple veins, pinnatifid to pinnatisect, with spiny-dentate lobes [7]. Its flowers can be white, yellow, burgundy, red, or green [4]. *G. tournefortii* has been used to make traditional recipes and has been mentioned in local

* Correspondence to: Faculty of Medicine and Health Sciences, An-Najah National University, P.O. Box 7, Nablus, Palestine.
E-mail address: j.amer@najah.edu (J. Amer).

https://doi.org/10.1016/j.biopha.2022.113885
Received 4 August 2022; Received in revised form 13 October 2022; Accepted 14 October 2022
Available online 18 October 2022

folkloric songs and sayings [7]. Its use in food is very ancient; it was cited more than 2000 years ago in the Babylonian Talmud and other Biblical writings [8]. According to al-Muqaddasi, a Jerusalem geographer, *G. tournefortii* was one of the plant species that Palestine was privileged with. Excessive *G. tournefortii* gathering for commercial purposes decreased availability; thus, its gathering was limited to domestic use [9].

The stems, flowers, leaves, and seeds of *G. tournefortii* can be used as food. In Palestine, Jordan, and Syria, the tender plants' flower buds are collected and cooked before flowering [4,5]. In Turkey, the dried plant is stacked for winter food; the latex is used to make chewing gum, and the seeds are used as coffee [10]. In folk medicine, the plant stalk is considered hepatoprotective and a blood purifier. In Iran, its latex is used for burning off warts and drying up sores, and in Lebanon as an emetic and a cure for snakebite [4,5]. In traditional medicine, the plant is used to treat kidney diseases, anorexia, heart stroke, chest pain, gastric inflammation, diarrhea, bronchitis, gingivitis, vitiligo, and diabetes [4]. The *G. tournefortii* plant has numerous phytochemical constituents in its aerial parts, roots, seeds, and flower buds. Researchers were mainly interested in the flower buds, from which many components were isolated using analytical methods. These include sterols (stigmasterol, B-sitosterol), tocopherols (α-tocopherol, β-tocopherol, α-tocotrienol, β-tocotrienol, δ- tocotrienol), fatty acids (arachidic, linolenic, stearic, oleic, palmitic), minerals (Ca, K, P, Mg, Na), crude protein, and water-insoluble fibers [11]. Other sterols isolated and identified include 5-avenasterol, campesterol, 7-stigmastenol, 7-avenasterol, and β-sitosterol, the most predominant. Vitamin E was also found in the oil [12]. Previously conducted studies revealed the presence of chlorogenic acid, gallic acid, caffeic acid, terpinen-4-ol, linalool, cymene, limonene, zingiberene, stigmasterol, β-sitosterol, aesculin, scopoletin and quercetin [11]. It has been reported that *G. tournefortii* possesses antibacterial and hypolipemic effects [12,13]. In addition, aerial parts of *G. tournefortii* demonstrated anti-inflammatory and anti-nociceptive effects in a mouse model [14], and hepatoprotective effects were shown in carbon tetrachloride-induced hepatotoxicity in rats [15].

One of the fundamental features of cancer is tumor clonality, *i.e.*, the development of tumors from single cells that begin to proliferate abnormally [16–19]. This process can be retarded by apoptosis, cytotoxicity, and antiproliferative activity [20]. According to 2018 WHO statistics, liver cancer was among the leading causes of cancer mortality, with 782,000 deaths by the end of that year [21]. For these reasons, and in addition to the wide use of this plant in Palestine, we aimed to discover part of its anti-hepatocellular cancer activity *in vivo* and *ex vivo* models, specifically in its flowering bud part. The hepatocellular cancer mouse model (hepatocellular carcinoma) mimics liver cancer in human patients. Thus, evaluating the effect of *G. tournefortii* extracts in this preclinical model could greatly benefit the assessment of its effect on inflammatory and molecular biology systems and its potential impact as a supplementary treatment for liver diseases.

2. Materials and methods

2.1. Plant material and extraction method

The fresh flowering buds of *G. tournefortii* were purchased in local Palestinian markets in Nablus. The plant was taxonomically characterized in the Pharmacognosy Laboratory at An-Najah National University and given the specimen code Pharm-PCT-1133. The fresh plant sample was washed several times using distilled water to remove contaminants. The cleaned flowering buds of *G. tournefortii* (200 g) were cut into small pieces and boiled in a beaker with 1 L of distilled water for 30 min. The boiled mixture was filtered using a Buchner funnel, and the extract of the sample was lyophilized into a powder using a freeze drier. For cytotoxicity assessment, *G. tournefortii* extracts were diluted in sterile water to a concentration of 100 mg/ml. Cytotoxicity was evaluated in primary isolated hepatocytes from HCC mice and compared to those from mice that received the vehicle.

2.2. HCC mouse model

Male mice of NOD.CB17-Prkdc-SCID/NCrHsD background (severe combined immune deficient mice) [22], 12 weeks of age, weighing 22 ± 0.5 g, received care according to the ethics regulations of the An-Najah National University and NIH guidelines. All animal protocols were approved by the institutional animal care ethical committee at the An-Najah National University (Ref: Med. Oct/2018/59) and housed in a barrier facility (Supplementary 1 showing ethical approval). For the xenograft model, 6×10^6 Hep3B cells (human liver hepatocellular carcinoma cell line) /100μl were injected subcutaneously on the back (N = 10 animals). Tumor weight and volume and mice weight were monitored daily macroscopically for 12 days from day two following cell injection. On day 10, one group was injected i.p. with *G. tournefortii* extracts dissolved in water at a dose of 60 mg/kg body weight, and another group received only the vehicle (100 % water) (N = 10 per group). For tumor serum marker measurements, tail blood was drawn every two days starting on day two after the Hep3B injection. At sacrifice (day 12), tumors were collected to determine weight and volume, and livers were collected for molecular biology and histopathology analyses. The animals were sacrificed by intramuscular injection of 0.1 ml of ketamine: xylazine: acepromazine (4:1:1) per 30 g of body weight before cervical dislocation.

2.3. Histological assessments of liver injury

The posterior one-third of the liver was fixed in 4 % formalin for 24 h and then paraffin-embedded in an automated tissue processor. Section (7 mm) were stained for H&E to evaluate steatosis, necro-inflammatory regions, and apoptotic bodies.

2.4. Immunofluorescence (IF) staining of liver macrophages

For deparaffinization, paraffin-embedded sections were placed in bath at 60 °C for 15 min, incubated in xylene at room temperature for 15 min, and then transferred sequentially into 100 % EtOH, 95 % EtOH, 70 % EtOH, and 50 % EtOH for 4 min each at room temperature. Sections were rinsed in deionized water and stored in PBS. For antigen retrieval, we used a buffer (10 mM citrate, pH 6.2, 2 mM EDTA, and 0.05 % Tween 20). Liver tissue samples were outlined with 100 μl of KASBLOCK liquid blocker to minimize the volume of antibody solution needed for staining. Samples were incubated overnight at 4 °C with rabbit anti-mice F4/80 (diluted 1:30; Ab6640, Abcam). Samples were washed with PBS, secondary antibodies conjugated with Cy-2 were applied for one hour at room temperature, and image capture was performed. Samples were viewed and imaged with a Zeiss LSM 710 confocal laser scanning system (Zeiss, Germany) attached to a Zeiss Axiovert 135 M microscope equipped with a Plan-Apochromat Zeiss 63X lens. An argon laser (488 nm excitation) was used to detect green fluorescence, and an Alexa Fluor laser (552 nm) was used to detect red fluorescence. IF quantitation was assessed by counting F4/80 stained cells per field. Averages of 10 fields were calucaulted.

2.5. RNA isolation, cDNA preparation, and real-time PCR

Total cellular RNA was isolated from liver tissue with 2 ml TRI Reagent (Bio LAB; Cat# 90102331) per cm^3 of tissue. Samples were homogenized for ten minutes at room temperature. 200 μl chloroform (Bio LAB; Cat# 03080521) was added to each sample, incubated for 10 min at room temperature, and centrifuged (1400 rpm) for 15 min at 4 °C. For RNA precipitation, the supernatant from each sample was transferred to a new micro-centrifuge tube, 0.5 ml of isopropanol (Bio LAB; Cat# 16260521) was added and incubated for ten minutes at 25 °C. The tubes were then centrifuged (12,000 rpm) for ten minutes at 4 °C. The

supernatants were removed, and 1 ml of 75 % ethanol was added to the pellet and centrifuged (7500 rpm) for five minutes. The pellets were air-dried at room temperature for 15 min, 50 μl of DEPC was added, and the samples were heated for ten minutes at 55 °C. Liver RNA was extracted as described above. Preparation of cDNA was performed with a high-capacity cDNA Isolation Kit (R&D; Cat# 1406197). Real-time PCR was performed with TaqMan Fast Advanced Master Mix (Applied Biosystems; Cat# 4371130) to quantify HNF4A, FOXA-3,VEGF, TGF-β, TIMP-1, MKI67, PDGFRA, and CDKN2A gene expression, normalized to the expression of the housekeeping gene GAPDH.

2.6. Serum tumor markers

Quantitative measurements of mouse serum of α-fetoprotein (Abcam; Ab 210969) and Glypican-3 (MyBioSource, Inc; USA) were determined by ELISA according to the manufacturer's instructions.

2.7. Primary hepatocytes isolation

Briefly, the abdominal area was cleaned with 70% alcohol, and a midline incision exposed the abdominal site. Livers were perfused from the catheter into the portal vein with a pump at a rate of 4.5 ml/minute with perfusion medium (ThermoFisher, Cat # 17701–038) and later for another 6–7 min with liver digest medium (ThermoFisher, Cat # 17703–034). The livers were then placed in a 100 mm plate filled with cold 20 ml washing medium, cut into pieces, and transferred through 100/70 μm filters into 50 ml centrifuge tubes. The cells were centrifuged at 50× g for 3 min at 4 °C. The supernatant was discarded, and 20 ml 40 % cold Percoll (Sigma P1644–500 ml) was added to each tube. After centrifugation at 150–200× g for 7 min at 4 °C viable hepatocytes were collected from the bottom of the tubes. Washed hepatocytes were cultured in a collagen-coated plate at a concentration of 2.2×10^5 /ml in 6-well plates. Cells were incubated at 37 °C and 5 % CO_2 for 2.5–3.5 h, washed once to remove dead cells, and fresh medium was added for an additional 24 h. The next day, the medium was changed, and the hepatocytes were used for the experiments. Hepatocyte conditioning was accomplished with Williams E medium (ThermoFisher, Cat number: A1217601) supplemented with 6% FBS, glutamine, dexamethasone, glucagon, and insulin. For *in vitro* assays, *G. tournefortii* extracts dissolved in water were incubated with the primary hepatocytes from the HCC mice (10^6/ml) in concentrations of 50, 100, and 200 μg/ml for 24 h at 37 °C. The viability of hepatocytes was determined by trypan blue staining. Briefly, 100 μl of cells were aseptically transferred to a 1.5 ml tube and incubated for 3 min at room temperature (25 °C) with an equal volume of 0.4 % (w/v) trypan blue solution (Sigma, USA). Cells were counted using a dual-chamber hemocytometer and a light microscope. Nonviable cells were stained blue and viable cells were unstained. These two types of cells were recorded separately, and the mean of six independent cell counts was pooled for analysis.

2.8. 3D Cancer spheroids capacity test

Hep3B cells (4000 cells) were cultured in ultra-low attachment round bottom 96-well plates (Corning, Life sciences) in the presence of 100 μg/ml *G. tournefortii* for 24 h. Doxorubicin, 100 μg/ml, was used as a positive control. Images of spheroids or aggregates were taken at time zero and after 24 h using an inverted microscope at a 100x maximal magnification. Images were analyzed using ImageJ software.

2.9. Flow cytometry analysis

Harvested primary hepatocytes were diluted to 10^6/ ml in staining buffer (1% bovine albumin in saline). For signaling pathway proteins, cells were incubated with rabbit anti-mouse for phosphorylated p53/p-AKT/PI3Ks, and mTOR (R&D System, Minneapolis, MN) diluted at 1:1000 overnight at 4 °C, followed by peroxidase-conjugated anti-rabbit (Abcam, Israel, diluted 1/5000), for 45 min at room temperature. For viability and apoptosis measurement, staining of fragmented DNA with propidium-iodide (PI) and staining of phosphatidylserine with annexin V-conjugated to FITC was performed according to the manufacturer's instructions (R&D System, Minneapolis, MN). Apoptosis was defined as annexin-V^+ and PI^-. Viable cells were defined as annexin-V^- and PI^-. Unstained controls, such as IgG isotype and FMO, were added to all experiments. Staining with PI was used to analyze the cell cycle by quantitating DNA content following incubation with *G. tournefortii*. Fixation of the primary hepatocytes from the HCC animals was performed in cold 70% ethanol at 4 °C for at least 30 min. The cells were then washed 2× in PBS at 2000 rpm. To confirm that only DNA was stained, the cells were treated with ribonuclease (50 μl of 100 μg/ml RNase). The cells were then stained with 5 μl of 50 μg PI/100 ml and analyzed by flow cytometry (Becton-Dickinson LSR II, Immunofluorometry systems, Mountain View, CA).

2.10. Proliferation assay

Primary hepatocytes were isolated and washed following harvesting and stained with CFSE (5,6-carboxyfluorescein diacetate) according to the manufacturer's protocol (Invitrogen, Oregon). Briefly, 5 μM CFSE staining was incubated with 10^6 liver hepatocytes in cell culture. CFSE labeling is extremely fluorescence. The majority of CFSE initially taken up by the cells is lost within the first few days following proliferation, five days on our case. Loss of fluorescence reflect higher proliferation. The units obtained are the Mean Fluorescence Intensity (MFI- arbitrary unit). Results were calculated as the fold change in MFI at day 5 as compared to day zero and analyzed by LSR-Fortezza. For cell viability measurements, trypan blue negative cells (viable cells) were counted using light microscopy and calculated as the following equation:

Viable cells (%) = total number of viable cells per ml/total number of cells per ml x100

2.11. Oxidative assay

Lipid peroxidation was estimated by measuring thiobarbituric acid-reactive substances (TBARS) expressed in terms of malondialdehyde (MDA) content. The MDA values were calculated using 1,1,3,3-tetraethoxypropane as standard and expressed as nmol of MDA/g. Glutathione (GSH) was measured as reported [23]. The supernatant (200 μl) was added to 0.25 M sodium phosphate buffer (1.1 ml, pH 7.4), followed by the addition of DTNB 0.04 % (130 μl). The mixture was brought to a final volume of 1.5 ml with distilled water, and absorbance was read in a spectrophotometer at 412 nm; results were expressed as μg GSH/μg protein. The activity of superoxide dismutase (SOD) was measured by monitoring its ability to inhibit the photochemical reduction of nitro blue tetrazolium (NBT). Each reaction mixture (1.5 ml) contained 100 mM Tris/HCl (pH 7.8), 75 mM NBT, 2 μM riboflavin, 6 mM EDTA, and 200 μl of supernatant. The production of blue formazan was monitored by absorbance at 560 nm. One unit of SOD is defined as the quantity required to inhibit the rate of NBT reduction by 50 %. The rate of H_2O_2 decomposition was monitored by absorption at 240 nm. One unit of CAT activity is defined as the number of enzymes required to decompose 1 μM of hydrogen peroxide in 1 min.

2.12. Western blot analysis

Primary hepatocytes protein extracts were prepared in hepatocytes liver homogenization buffer (50 mmol/L Tris–HCl [pH 7.6], 0.25 % Triton-X 100, 0.15 M NaCl, 10 mM $CaCl_2$ and complete mini EDTA-free protease inhibitor cocktail (Roche Diagnostics, Mannheim, Germany). Next, proteins (30 μg per lane) were resolved on a 10% (w/v) SDS-

polyacrylamide gel (Novex, Groningen, The Netherlands), under reducing conditions. For immunoblotting, proteins were transferred to a Protran membrane. Blots were then incubated for 1 h at room temperature in a blocking buffer containing 5 % skim milk (w/v). Next, the blots were incubated with rabbit anti-mouse p53/p-AKT(S473)/ p-PI3K (T180/Y182) and anti-human/mouse/rat AKT/PI3K (R&D System, Minneapolis, MN) diluted 1:1000 overnight in 4 °C, and subsequently, with peroxidase-conjugated with Anti-rabbit (Abcam, Israel, diluted 1/5000), for 1.5 h at room temperature. Immunoreactivity was detected using an ECL kit (Abcam, Israel).

2.13. Statistical analysis

Statistical differences were analyzed with a 2-tailed unpaired Student's t-test (for comparison between two groups) or two-way analysis of variance (two-way ANOVA with Newman-Keuls' for multiple groups) using Graph Pad Prism 5.0. Data are shown as means ± SEM.

3. Results

3.1. G. tournefortii extracts decreased tumor mass and partly maintained liver histological characteristics in animals with hepatocellular carcinoma (HCC)

The HCC model was used to study tumorigenicity outcomes. The anticancer effects of *G. tournefortii* were evaluated by injecting the extracts. Tumor weight and volume were determined at the end of the experiment following Hep3B (HCC)-injections (Fig. 1 A). The tumor size of HCC mice receiving the *G. tournefortii* extract was 0.9 ± 0.1 cm, and the size in mice receiving the vehicle was 2.0 ± 0.6 cm. Fig. 1B shows the gradual increase in tumor size following HCC injections. On day 10, each group was split into two; one group received the vehicle and the second group received *G. tournefortii* extract. On day 12, tumor size continued to increase in mice treated with the vehicle, while mice that received the *G. tournefortii* extract showed a significant decrease in tumor size ($p = 0.01$). The average tumor weight (Fig. 1 C) and volume (Fig. 1D) are presented. Data show a reduction in tumor weight (5-fold) and tumor volume (2-fold) following *G. tournefortii* extract injection ($P < 0.01$). To investigate if *G. tournefortii* extracts can induce changes in

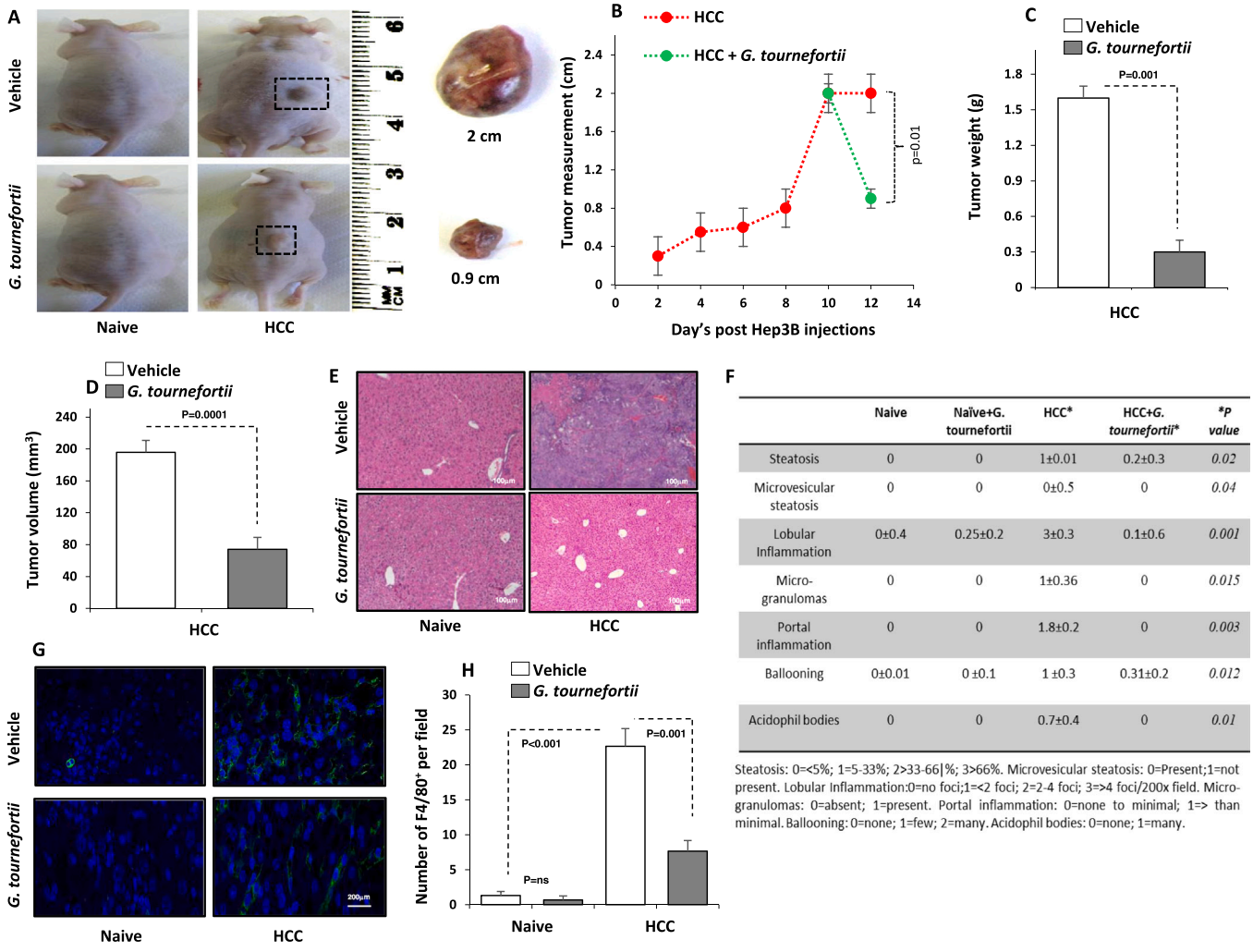

	Naive	Naïve+G. tournefortii	HCC*	HCC+G. tournefortii*	*P value
Steatosis	0	0	1±0.01	0.2±0.3	*0.02*
Microvesicular steatosis	0	0	0±0.5	0	*0.04*
Lobular Inflammation	0±0.4	0.25±0.2	3±0.3	0.1±0.6	*0.001*
Micro-granulomas	0	0	1±0.36	0	*0.015*
Portal inflammation	0	0	1.8±0.2	0	*0.003*
Ballooning	0±0.01	0 ±0.1	1 ±0.3	0.31±0.2	*0.012*
Acidophil bodies	0	0	0.7±0.4	0	*0.01*

Steatosis: 0=<5%; 1=5-33%; 2>33-66|%; 3>66%. Microvesicular steatosis: 0=Present;1=not present. Lobular Inflammation:0=no foci;1=<2 foci; 2=2-4 foci; 3=>4 foci/200x field. Micro-granulomas: 0=absent; 1=present. Portal inflammation: 0=none to minimal; 1=> than minimal. Ballooning: 0=none; 1=few; 2=many. Acidophil bodies: 0=none; 1=many.

Fig. 1. *G. tournefortii* ameliorates liver injury and tumor parameters in the HCC mouse model. (A) Representative pictures of mice displaying tumors at the back of the animals. Tumors extracted were measured at the end of the sacrifice day. Vehicle-treated mice show no evidence of tumors, and livers are macroscopically normal. Tumors removed from HCC mice measured 2 cm compared to 0.9 cm of those extracted from mice receiving *G. tournefortii.* (B) Kinetic measurements of tumor size. (C) tumor weight and (D) tumor volume were measured on the back of the mice. (E) H&E staining of liver sections. (F) Quantitation of liver histology is summarized and represented as average ± SEM (n = 10 mice per group). (G) Confocal microscopy of F4/80^{+} expression on macrophages from liver sections (63× resolution). (H) Averages of 10 fields of the number of F4/80^{+} cells/field in HCC mice with and without *G. tournefortii.* Experiments were repeated three times. Data are shown as means ± SEM.

liver histology, we stained mouse liver biopsies with H&E. The mice treated with the vehicle or naïve mice that received the *G. tournefortii* extracts showed no histopathological effect on the liver tissue (Fig. 1E). However, the HCC-implanted mice exhibited hemorrhage, necrosis, dysplasia, steatosis, lobular inflammation, and hepatic cell carcinoma. The HCC-implanted mice injected with the *G. tournefortii* extract showed a significant reduction in these markers (Fig. 1F). HCC progression is known to be driven by chronic inflammation. Macrophages play a crucial role in chronic liver inflammation [24], and the tumor microenvironment, which plays a key role in the progression of HCC, contains abundant tumor-associated macrophages [25]. As the role of macrophages in the development and progression of HCC has been recognized [26], we stained macrophages from liver mouse tissue and examined them by immunofluorescence using confocal microscopy. Images show a few F4/80-positive macrophages in liver sections obtained from either naïve mice treated with vehicle or naïve mice treated with the *G. tournefortii* extract (Fig. 1G). In contrast, HCC mice exhibited high F4/80-positive infiltrates, which diminished after treatment with the *G. tournefortii* extract (Fig. 1G). Low numbers of F4/80^{+} were observed in liver biopsies of HCC mice treated with the *G. tournefortii* extract compared to their untreated counterparts, indicating fewer infiltrated macrophages and a reduced inflammatory response (Fig. 1H, P = 0.001).

3.2. Tumor markers and molecular characteristics of G. tournefortii-treated HCC mice

The vascular endothelial growth factor (VEGF) is a growth factor with important pro-angiogenic activity, with a mitogenic and anti-apoptotic effect on endothelial cells. Among its activities, it increases vascular permeability and promotes cell migration, thus actively contributing to regulating the normal and pathological angiogenic processes [27]. In addition, the transforming growth factor β (TGF-β) signaling pathway plays an essential role in many biological processes, including cell growth, differentiation, apoptosis, migration, and cancer initiation and progression [28]. Tissue inhibitor of metalloproteinase (TIMP-1) is a prognostic marker for the progression and metastasis of colon cancer through the FAK-PI3K/AKT and MAPK pathways [29]. We sought to study the mechanisms of these pro-carcinogenic regulatory genes in the HCC- mice treated with *G. tournefortii*. Expression levels of VEGF, TGF-β and TIMP-1 genes were determined by RT-PCR as

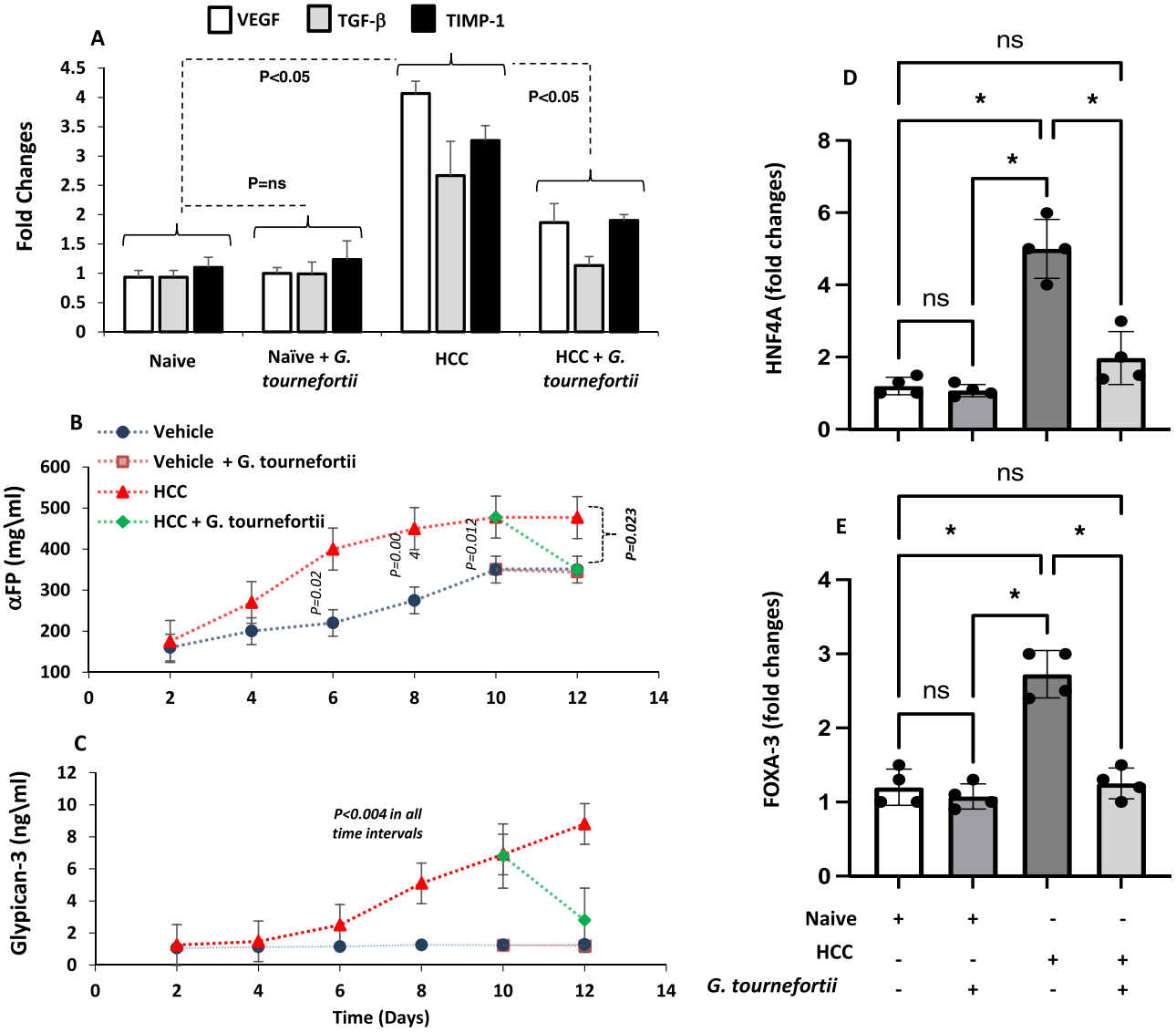

Fig. 2. Genetic and serum tumor markers in HCC mice receiving *G. tournefortii* extracts. (A) VEGF, TGF-β and TIMP-1 gene expression levels were assessed by RT-PCR. Gene expression was normalized to the expression of the housekeeping gene GAPDH. The kinetic measurements of serum (B) αFP and (C) Glypican-3 were determined by ELISA. RT-PCR of the regulatory gene markers of (D)HNF4A (E) and FOXA-3 were assessed in mice livers. Experiments were repeated three times. Data are shown as means ± SEM. N = 4 in each group.

described in Methods. Fig. 2A displays the mRNA levels of all genes elevated in the HCC mice. Elevation of these genes was slowed following *G. tournefortii* treatment of the HCC mice ($P < 0.05$). To further characterize HCC mice treated with *G. tournefortii* extracts, we measured αFP and Glypican-3 (GPC3) to assess the extent of malignant cells. GPC3 is a heparan sulfate proteoglycan anchored to the plasma membrane that interacts with growth factors and modulates their activity [30]. It has also been shown that soluble GPC3 and αFP can detect well or moderately differentiated HCC [30]. Simultaneous determination of GPC3 and αFP improves overall sensitivity from 50 % to 72 % [31]. Following HCC implantation, there is a gradual increase in serum αFP and GPC3 during tumor progression (Fig. 2B-C). On day 12, *G. tournefortii* extracts caused a remarkable reduction in serum αFP and GPC3 levels in the HCC mice to levels comparable to mice treated with vehicle ($P < 0.01$).

In an attempt to clarify the direct evidence on the regulation relationship between the *G. tournefortii* and αFP and GPC3, we assessed hepatocyte nuclear factor-4-alpha (HNF4α) and Hepatocyte Nuclear Factor 3-Gamma (FOXA-3). HNF4α has been well recognized as an important transcription factor that regulates gene expression involved in the differentiation of liver and gastrointestinal cells [32], for instance, analyses of HNF4α null visceral endoderm found reduced or absent expression of αFP [33]. Additionally, FOXA-3 has been shown to promote the occurrence and development of HCC by up regulating αFP [34]. FOXA-3 shown to control transcription at the αFP and GPC3 locus in embryonic liver and showed a remarkable linear correlation [35]. Targeting FOXA-3 may be a valid treatment option for HCC patients [36]. Fig. 2D and E demonstrate 4-fold and 3.2-fold increase in HNF4α and FOXA-3 in the HCC mice model, respectively. Moreover, *G. tournefortii* extracts caused a notable reduction in HNF4α and FOXA-3 gene expressions from HCC livers to comparable levels to naive mice treated with vehicle ($P < 0.02$).

To deepen our study, we determined the molecular profiling and signaling in liver extracts by assessing gene expression profiling known as differentially regulated in HCC; some of these genes play a significant prognostic role [37]. MKI67 expression, found under normal conditions only in proliferating cells [38], was determined by RT-PCR. PDFGRA functions as a tyrosine kinase receptor and is important for transmitting signals within a cell for signal transduction and regulation of cellular behavior, such as cell division [39]; CDKN2A controls the cell cycle [40]. Quantitation of phosphorylated proteins by flow cytometry analysis was also performed. The tumor suppressor p53 is one of the most frequently mutated genes in liver cancer. p53 regulates the expression of genes involved in cell cycle progression, cell death, and cellular metabolism to avert tumor development due to carcinogens [41]. The intracellular pathway of protein kinase B (PKB), also known as AKT, was evaluated. AKT plays a crucial role in multiple cellular processes, such as glucose metabolism, apoptosis, cell proliferation, transcription, and cell migration [42]. Phosphoinositide 3-kinases (PI3Ks) and mTOR involved

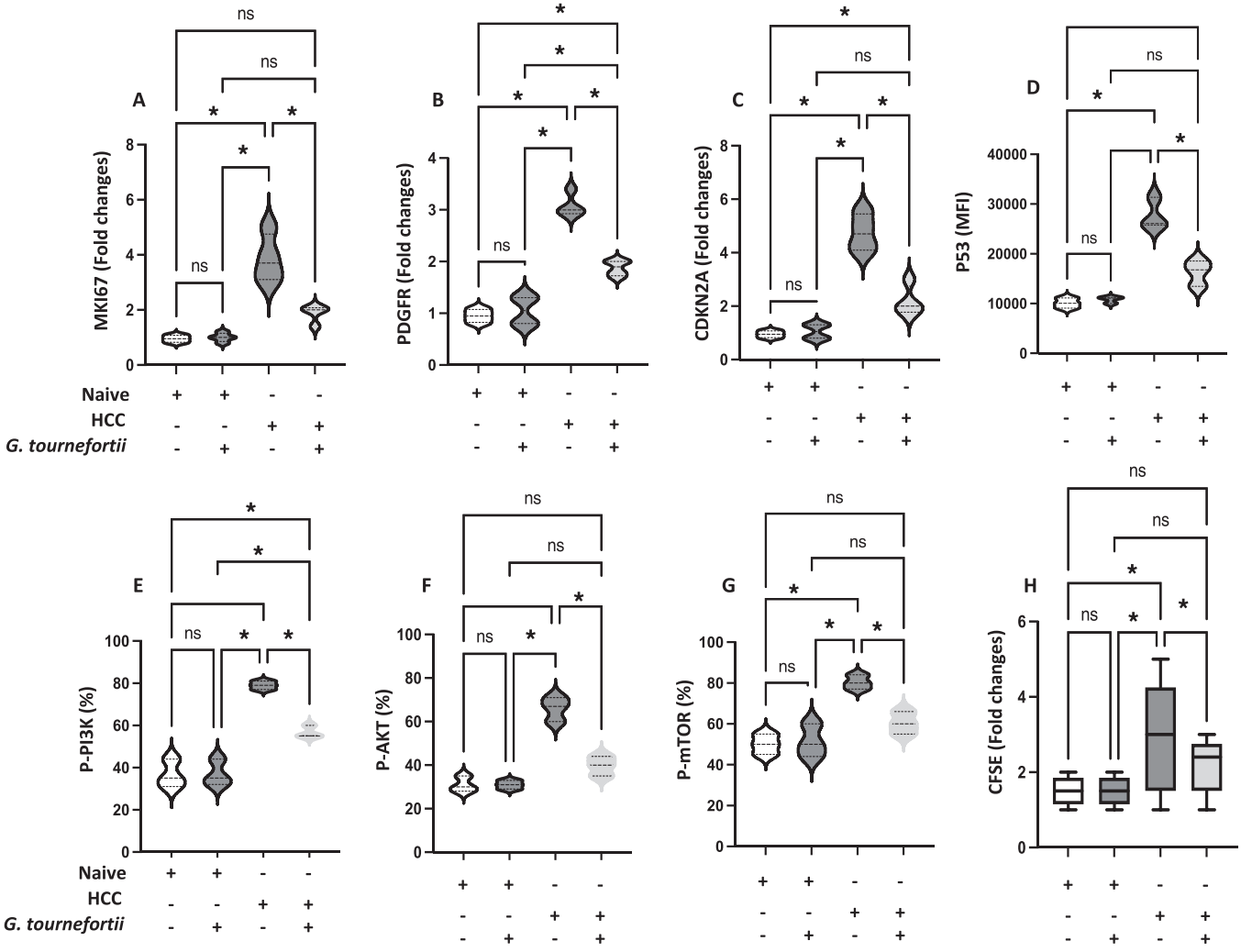

Fig. 3. Molecular characteristics of HCC mice that received *G. tournefortii* extracts. RT-PCR analysis of primary hepatocytes gene expression of (A) MKI67 (B) PDGFRA (C) CDKN2A (D) p53 and flow cytometry analysis of phosphorylated signaling pathway of (E) PI3K (T180/Y182) (F) AKT (S473) and (G) mTOR were determined. (H) CFSE proliferation marker analysed by flow cytometry. All experiments were repeated four times; averages ± SD are presented.

in cellular functions such as cell growth, proliferation, differentiation, motility, survival, and intracellular trafficking, which in turn are involved in cancer [43,44], were also assessed.

Fig. 3 A, B, and C show the RT-PCR of MKI67, PDFGRA, and CDKN2A, respectively. The results demonstrate a significant increase in MKI67 (3.75-fold), PDFGRA (3.2-fold), and CDKN2A (4.8-fold) in the HCC mice compared to the naive mice. HCC mice treated with *G. tournefortii* extracts showed a lower expression of all tested genes compared to the HCC mice ($P < 0.05$), and inhibited expression of MKI67 was similar to gene expression in naive mice ($P = ns$). The *G. tournefortii* treatment results in the naïve mice were similar to their untreated counterparts. Flow cytometry analysis of p53, p-PI3K, p-AKT, and p-mTOR are presented in Fig. 3D-G. Data demonstrate elevated mean fluorescence intensities (MFI) of p53 protein and elevated phosphorylated AKT/ PI3K/ mTOR percentages in the primary hepatocytes obtained from liver extracts. These phosphorylated signaling proteins were decreased in the primary hepatocytes of HCC mice receiving *G. tournefortii* ($P < 0.05$) in P53 and p-PI3K, and lower expression was detected in p-AKT and p-mTOR ($P = ns$) in comparison to naïve mice. No effect of *G. tournefortii* extracts was observed in naïve mice with or without treatment. The above selected proteins were also assessed through the western blot analysis confirming same patterns of results obtained *via* the flow cytometry method (Supplementary 2). The assessed genes clearly indicated modulatory effects of *G. tournefortii* extract on HCC proliferation and were confirmed through CFSE staining; proliferative marker, as described in materials and methods. As shown in Fig. 3H, *G. tournefortii* extracts inhibited cell proliferation in primary hepatocytes to levels similar to naïve mice ($P = ns$). These results were associated with reduced viablitity of HCC cells treated with *G. tournefortii* extracts (dara not shown). Overall, the data show that *G. tournefortii* extracts modulated tumor progression by reducing signaling pathways of p53 and p-PI3K and delaying proliferation of the HCC (CFSE) and as represented by lower PDGFAR and CDKN2A. Moreover, *G. tournefortii* extracts inhibited MKI67, and p-AKT/p-mTOR signaling pathways, indicating its vital role in reducing cancer migration, invasion, and progression. For the first time, we report the effects of *G. tournefortii* in minimizing the development and metastasis of HCC.

3.3. *G. tournefortii inhibits the DNA cell cycle and increases the apoptotic and necrotic activity of HCC isolated primary hepatocytes in vitro*

Flow cytometry analysis of PI-stained nuclei cells was used to validate the ability of the *G. tournefortii* extract to induce disturbances in the cell cycle of HCC hepatocytes following CDKN2A gene alteration. The extract was diluted in sterile water before incubation with hepatocytes at 37 °C for 24 h at a concentration of 50, 100 and 200 μg/ml. The control cells were treated with water only. Doxorubicin (Dox) was used as a positive control to induce cell cycle progression [45].

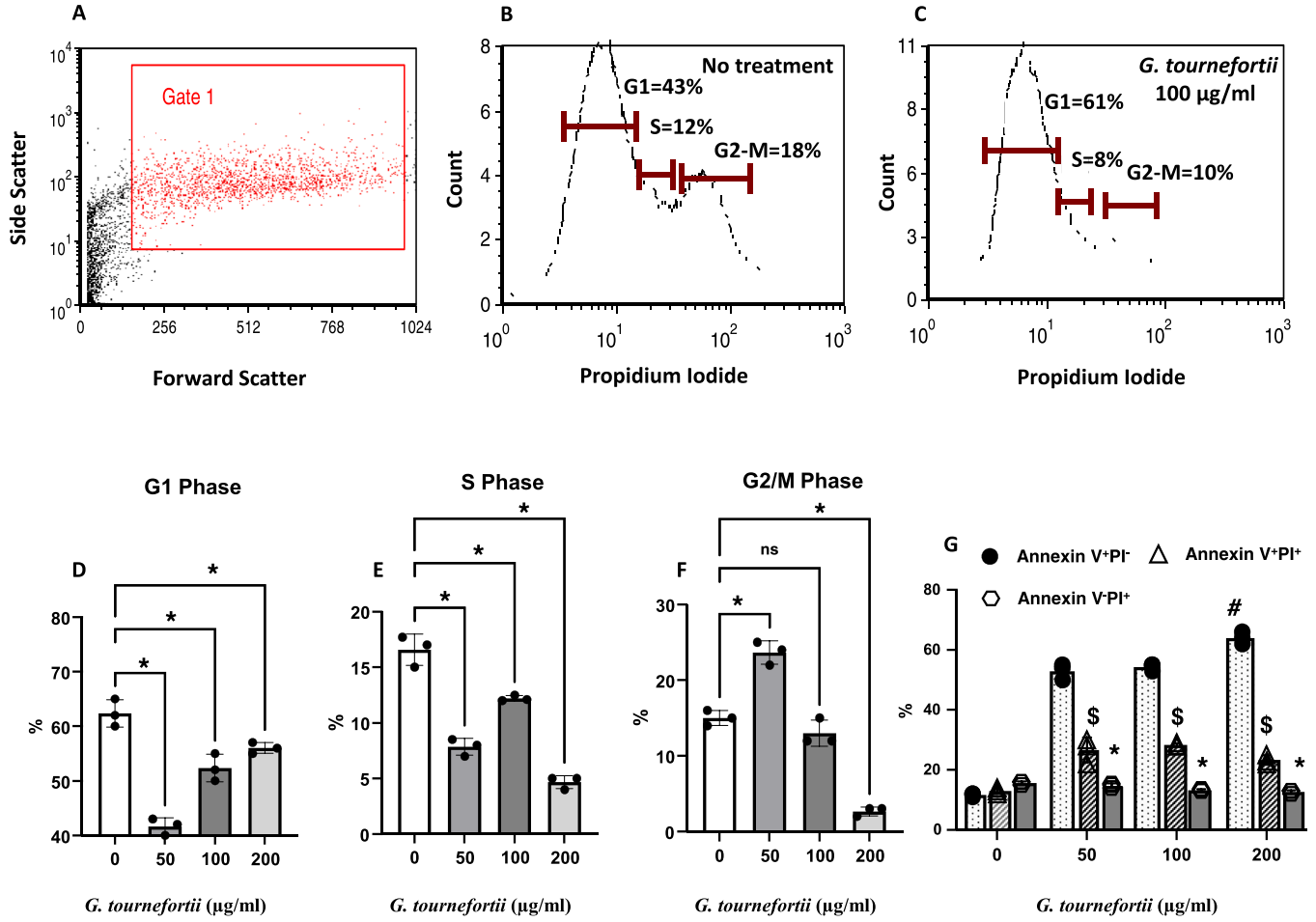

Fig. 4. *G. tournefortii* inhibited the G2/M phase of the cell cycle of primary hepatocytes and initiated cell apoptosis. (A) Representative dot plot and (B-C) histograms demonstrating the distribution of cell cycles. Averages of 3 different readings of (D) G1 phase, (E) S phase, and (F) G2/M phase following treatment with 50, 100, and 200 μg/ml *G. tournefortii* extract, [$*P < 0.05$]. (**G**) Average of the apoptotic and necrotic markers of primary hepatocytes obtained from HCC mice following treatment with *G. tournefortii*. Primary hepatocytes were treated with 50,100 and 200 μg/ml of *G. tournefortii* extracts. Apoptosis and necrosis averages ± SD are shown. For statistical differences, paired and unpaired student t-test and analysis of variance were used, [$^{*\#\$}P < 0.05$]. All the *in vitro* experiments were repeated 4 times.

Fig. 4 A shows a representative dot plot of cytometry analysis of primary hepatocytes according to their size (Forward Scatter) and granularity (Side Scatter). Gate 1 was set to include viable cells. Fig. 4B and C illustrate representative histograms of cell cycle analysis of G1, S and G2-M phases of untreated and *G. tournefortii* (100 μg/ml) treatment, respectively, as stained with PI.

The data in Fig. 4D shows a significant elevation in the proportion of cells in the G1 phase following treatment with the *G. tournefortii* extract. Average values of 52.53 ± 3.32 %, 56 ± 5.56 %, and 52.67 ± 4.04 % were obtained with 50, 100, and 200 μg/ml extracts, respectively, as compared to 41.6 ± 3 % in untreated samples ($P < 0.005$). There were no significant differences between the three different concentrations of the extract. A significant decrease in the S phase was seen following treatment with the extract at a concentration of 200 μg/ml (Fig. 4E). In addition, the three extract concentrations inhibited the HCC hepatocyte cell cycle in the G2/M phase to 3-, 6.8-, and 2.64-fold with 50, 100 and 200 μg/ml of *G. tournefortii* extract, respectively, as compared to untreated cells (Fig. 4F). These data show significant disturbance in cell cycle parameters in the G2/M phase (mitosis state) along with a significant shifting to the G1 phase (naive state), indicating a marked delay in the mitotic phase following *G. tournefortii* extract suggesting potential anticancer characteristics.

Phosphatidylserine (PS) is one of the phospholipid components of the cell membrane. Typically PS faces the cytoplasm, but in the case of apoptosis, a flipflop occurs, and PS faces the external surface of the cell [46]. To verify that *G. tournefortii* has an apoptotic effect in hepatocellular cancer cells from HCC mice, we used Annexin-V, a protein with a high affinity to phosphatidylserine, conjugated with FITC, to detect PS, and propidium iodide (PI) to identify necrosis, the last step of cell death. Early apoptosis was defined as Annexin-V^+PI^-; late apoptotic and necrotic cells as Annexin-V^+PI^+ and necrotic cells as Annexin-V^-PI^+. Three different concentrations of the *G. tournefortii* extracts were used (50, 100, and 200 μg/ml) to test a broad spectrum of apoptotic effects in the *in vitro* setting. Fig. 4G shows that 12.03 ± 4.2 % of untreated HCC hepatocytes underwent early apoptosis. Following treatment with 50, 100, and 200 μg/ml, the *G. tournefortii* extracts elevated apoptotic activity to 55.67 ± 4.4 %, 53.67 ± 4.4 %, and 62.67 ± 7.3 %, respectively ($P < 0.02$). Moreover, the *G. tournefortii* extracts decreased necrosis (Annexin-V^- and PI^+) and increased late apoptosis (Annexin-V^+ and PI^+) in a range of 1.8- to 2.6-fold increase ($P < 0.004$). These results suggest that *G. tournefortii* has anticancer properties, as revealed by increasing the apoptotic activity of hepatocellular cancer cells and thus shifting the cells to programmed cell death rather than causing necrosis.

3.4. Antioxidant properties of G. tournefortii

Free radicals and reactive oxygen species (ROS) are continually produced in the human body. These oxygen species are the primary source of cell damage and tumor cell progression. Therefore, to avoid damage, tissues are protected from oxidative injury through intracellular superoxide dismutase (SOD), glutathione peroxidase (GSH-Px) and catalase (CAT), and extracellular antioxidants (vitamins, antioxidants originated from herbs) [47]. Table 1 shows levels of serum and liver malondialdehyde (MDA, a lipid peroxidation marker), as well as serum and liver antioxidant enzymes of reduced glutathione (GSH), glutathione peroxidase (GPX), and catalase. Livers of HCC-induced mice treated with *G. tournefortii* extracts exhibited a significant increase of 1.28-, 1.25-, 1.22-, and 1.36-fold in serum GSH, SOD, CAT, and GSH-Px, respectively. A 1.57-fold decrease in MDA was obtained compared to HCC alone. Moreover, mouse livers from the HCC mice treated with *G. tournefortii* extracts showed elevated levels of GSH, SOD, CAT, and GSH-Px antioxidants by 1.3-, 1.4-, 1.5-, and 1.7-fold, respectively. These results show that the progress of liver injury is closely related to the downregulation of antioxidant enzymes in the liver, and *G. tournefortii* enhances the activity of these enzymes, alleviating liver cancer and counteracting hepatotoxicity.

3.5. G. tournefortii inhibited the Hep3B formation of 3D MCTS spheroids

Multicellular tumor spheroids (MCTS) are currently the most often used 3D tumor model in preclinical investigations and are widely accepted as a reliable tool for studying tumor behavior and drug testing [48]. The capacity of cells to form spheroids *in vitro* reflects increased tumorgenicity, enhanced proliferation potential, self-renewal and chemoresistance of cancer cells, and their ability to produce tumors *in vivo* [49–51]. Therefore, we investigated a possible role for *G. tournefortii* extract in altering the Hep3B spheroid formation capacity. Fig. 5A shows Hep3B cells forming a spheroid in untreated controls. In contrast, one large cluster of cells (white arrow) and many tiny clusters were formed in the presence of 100 μg/ml of *G. tournefortii* extract (Fig. 5B). In addition, a very large flat cluster and other smaller clusters were formed when treating Hep3B cells with doxorubicin (Fig. 5C). The number of cell clusters around the spheroid in the presence of *G. tournefortii* was significantly higher compared to the control (Fig. 5D). The circularity (Fig. 5E) and the area occupied by these cell clusters (Fig. 5F) were significantly reduced ($p < 0.05$). These results show that *G. tournefortii* inhibits spheroid formation suggesting a possible role in decreasing tumorgenicity and chemoresistance.

4. Discussion

Several studies have reported the anticancer properties of plants, including the *Gundelia* species [18]. However, these publications only presented one anticancer aspect and focused on testing the extract in an *in vitro* setting. The present report shows the anticancer effect on liver cancer in an *in vivo* animal model and in *ex vivo* hepatocellular carcinoma cells isolated from mouse livers. Other studies on the anticancer activity of *G. tournefortii* were conducted by Abu- Lafi et al. [51] and Betül Özaltun and Taner Dastan [52]. Abu-Lafi et al. found that methanol and hexane extracts of *G. tournefortii* showed anticancer properties against the HCT-116 cancer cell line. However, the water extract showed no significant effect. Betül Özaltun and Taner Dastan found that various concentrations of aqueous plant extracts obtained from different parts of the plant exhibited potent cytotoxic activity against human breast

Table 1
G. tournefortii affects serum and liver MDA, GSH, SOD, CAT, and GSH-Px levels. Data are presented as averages (n = 10) ± SD.

Group		MDA (nmol/g protein)	GSH (mg/mm protein)	SOD (Unit)	CAT (Unit)	GSH-Px (Unit)
Naive	Serum	4.28 ± 0.27	177.23 ± 10	231 ± 19	61.3 ± 3.5	50.32 ± 3.5
	Liver	3.18 ± 0.22	151.23 ± 8	216 ± 16	42.8 ± 6	40.23 ± 6
Naïve + G. tournefortii	Serum	5.22 ± 0.29	166 ± 9.3	245.2 ± 15	77.5 ± 3.6*	56.3 ± 6.5*
	Liver	3.22 ± 0.22	156 ± 10.2	223.9 ± 2	50.6 ± 7*	42.6 ± 3.3
HCC	Serum	8.9 ± 0.25*	122.3 ± 15*	144.5 ± 16*	42 ± 0.18*	31.2 ± 6*
	Liver	7.33 ± 0.5*	116.3 ± 9*	130 ± 9*	33.3 ± 0.25*	21.5 ± 6.3*
HCC + G. tournefortii	Serum	5.66 ± 0.16#	156.3 ± 9#	181.35 ± 8#	51.3 ± 5.1#	42.3 ± 1.3#
	Liver	4.1 ± 0.9#	147.35 ± 13#	177.9 ± 16#	48 ± 2.3#	36.25 ± 3.2#

* $P < 0.05$, compared with naïve group;
\# $P < 0.05$ with HCC group.

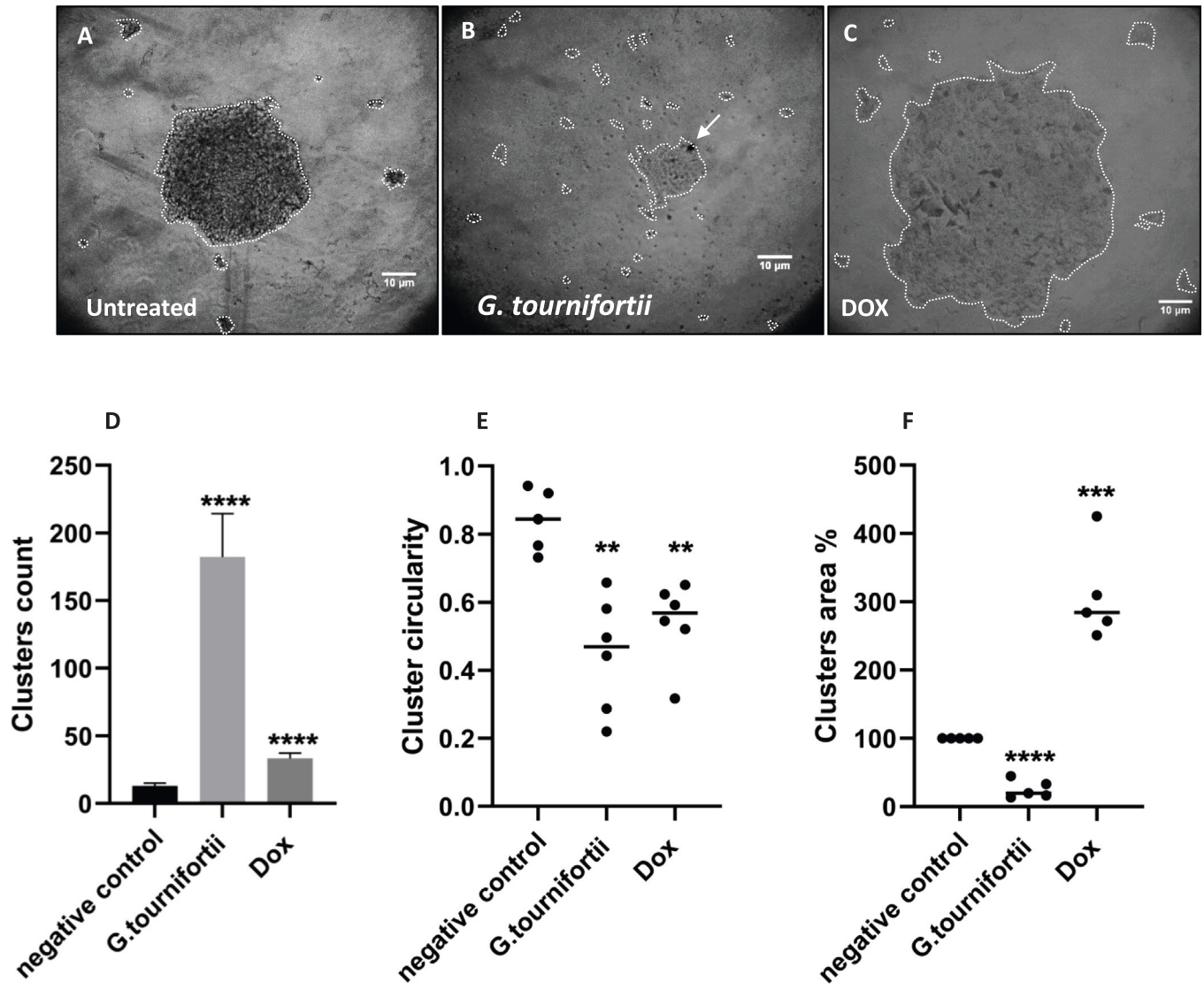

Fig. 5. *G. tournefortii* inhibited the formation of 3D MCTS spheroids. (A) Hep3B (HCC) spheroids formation capacity in untreated cells and in (B) the presence of *G. tournefortii* extract (100 µg/ml) after 24 h of treatment. (C) Doxorubicin (Dox) was used as a positive control (100 µg/ml). (D)The quantification of cluster count. The percentage of the occupied area by clusters compared to (E) control (F) and cluster circularity. A cell cluster contains at least 2–3 cells. Regarding circularity, the value of 1 denoted a perfect circle. The image's total magnification is 100x. Scale bar = 10 µm. Experiments were repeated three times. Data are shown as means ± SEM.

adenocarcinoma cells (MCF-7). Here, we choose to use *G. tournefortii* extracts in water solution to prevent any potential harm or hepatotoxicity from an organic solvent. We showed that the flower buds of *G. tournefortii* possess an anticancer agent that can act on several stages of the cell cycle: inhibition of p53 molecular expression, and cell proliferation through AKT/PI3K/mTOR, arresting the G2/M phase of mitosis and enhancing cell apoptosis. These antiproliferative effects could be partly explained as suppression of αFP and GPC3. AKT, also known as protein kinase B, plays a key role in cell proliferation, survival, and metabolism. AKT hyperactivation contributes to several pathophysiological conditions, including human cancers [53,54], and is closely associated with poor prognosis and chemo- or radiotherapeutic resistance [55]. Usually, AKT is activated by growth factors that activate PI3K and mTOR; here, it was inhibited following treatment with *G. tournefortii*.

High expression of CDKN2A was shown to promote proliferation and inhibit apoptosis of cancer cells, induce interstitial tumor angiogenesis, reduce the sensitivity of cancer cells to chemoradiotherapy, and ultimately affect the prognosis of HCC patients [56]. Moreover, the CDKN2A gene functions as a stabilizer of the p53 protein [57]. CDKN2A expression strongly correlated with diverse immune marker sets in HCC [58]. Our study suggests that CDKN2A expression potentially contributes to the regulation of tumor-associated macrophages (Fig. 1) and confirms previous data [58], suggesting its use as a prognostic biomarker for determining prognosis and immune infiltration in HCC. The effect of *G. tournefortii* on reducing the MKI67 gene expression could indicate its role in alleviating cancer cell migration, invasion, and progression. PDGFR-alpha is involved in tumor angiogenesis and maintenance of the tumor microenvironment and has been implicated in the development and metastasis of HCC [59]. Targeted inhibition of PDGFR-alpha, most probably through *G. tournefortii,* could be a rational strategy for the prevention and therapy of HCC.

Human hepatocellular carcinoma (HCC) is the most common primary malignancy of the liver [60,61] and represents a severe, worldwide threat to human health and quality of life. Patient survival after surgery remains relatively low, with 5-year survival rates after resection for early-stage disease ranging between 17% and 53% and recurrence rates as high as 70 % [61]. Therefore, it is essential to identify

biomarkers that reliably distinguish patients at high risk of recurrence. *G. tournefortii* could contribute to the medicinal treatment of liver cancer and be used as an AKT inhibitory agent, thus interfering with cell signaling responses and cycle checkpoints. In our study, we demonstrate the capacity of Hep3B to form spheroids *in vitro*, indicating the impact of *G. tournefortii* in modulating tumor behavior and minimizing proliferation potential, self-renewal, and chemoresistance of cancer cells. Various similar studies pointed to the importance of spheroid formation and the relevance of its inhibition to reduce tumorigenicity and chemoresistance [62–65]. Our results (Fig. 5) were consistent with the effects obtained from the signaling pathways (Fig. 3). Moreover, the anticancer effects of *G. tournefortii* extracts were associated with their antioxidant properties, as shown by the lower serum and liver MDA (a marker of lipid peroxidation) levels in the HCC model. The significant increase in hepatic lipid peroxide in mice explains the observed leakage of cellular ALT, AST, and ALP to the circulation due to liver injury (data not shown). On the other hand, *G. tournefortii* restored antioxidant levels (GSH, SOD, CAT, GSH-Px) in the serum and liver of the HCC mice. These data show that *G. tournefortii* has free radical scavenging activity, which could exert a beneficial action against pathological alterations caused by HCC.

5. Conclusions

G. tournefortii extracts suppressed cell proliferation and induced apoptosis in primary liver hepatocytes isolated from HCC mice by inhibiting AKT, PI3K, and mTOR phosphorylation. *G. tournefortii* showed to reduce HNF4α and FOXA-3 expressions and consequently this could in part explain inhibited expressions of αFP and GPC3 determine in serum of treated mice and confirmed the decrease in HCC proliferations. Gene expression of MKI67 and PDGFRA and the formation of 3D MCTS were inhibited. Moreover, treatment with *G. tournefortii* extracts significantly delayed the G2/M phase of the cell cycle progression and shifted the cells to the G1 phase through inhibited expressions of CDKN2A in association with the inhibitory expression of p53 in the tumor. Our findings suggest that the *G. tournefortii* extracts has the potential to be considered an anticancer treatment. This is the first report concerning the effect of *G. tournefortii* extracts in an animal model of liver cancer.

Funding

Not applicable.

CRediT authorship contribution statement

Johnny Amer: Conceptualization, writing—original draft preparation, validation, resources, and funding acquisition. **Ahmad Salhab**: Methodology, data curation, validation, formal analysis, and writing—review and editing. **Nidal Jaradat**: data curation, methodology. **Samer Abdallah**: Methodology and validation. **Hanood Aburas**: investigation. **Suhaib Hattab**: investigation. **Mustafa Ghanim**: formal analysis, and supervision. **Maliq Alqub**: Data curation. All authors have read and agreed to the published version of the manuscript.

Declaration of Competing Interest

The authors declare no conflict of interest.

Data availability

Data will be made available on request.

Acknowledgments

We would like to thank Prof. Rifaat Safadi; Head of Liver Institue at Hadassah Medical Center for assisting in research concept. Dr. Rasha Khayyat, Director of Medical Scientific Research Unit, An-Najah National University and Mr. Mohammad Arar from the Faculty of Pharmacy from An-Najah National University for the reagents supply and orders.

Institutional Review Board Statement

The animal study protocol was approved by the Ethics Committee of An Najah National University-Nablus (007/2020).

Informed Consent Statement

Not applicable.

Appendix A. Supporting information

Supplementary data associated with this article can be found in the online version at doi:10.1016/j.biopha.2022.113885.

References

[1] C. Aschwanden, Herbs for health, but how safe are they? Bull. World Health Organ. 79 (2001) 691–692.
[2] T. Mainardi, et al., Complementary and alternative medicine: herbs, phytochemicals and vitamins and their immunologic effects, J. Allergy Clin. Immunol. 123 (2009) 283–294.
[3] S.R. Groden, et al., Use of complementary and alternative medicine among older adults: differences between baby boomers and pre-boomers, Am. J. Geriatr. Psychiatry 25 (2017) 1393–1401.
[4] M. Asadi-Samani, et al., Gundelia: a systematic review of medicinal and molecular perspective, Pak. J. Biol. Sci. 16 (2013) 1238–1247.
[5] S. Lev-Yadun, et al., Traditional use of A′kub (*Gundelia tournefortii*, Asteraceae), in Israel and the Palestinian authority area, Econ. Bot. (1999) 217–219.
[6] S. Ceylan, et al., Antibacterial and antioxidant activities of traditional medicinal plants from the Erzurum region of Turkey, Ir. J. Med. Sci. (2019) 1–7.
[7] M.S. Ali-Shtayeh, et al., Traditional knowledge of wild edible plants used in Palestine (Northern West Bank): a comparative study, J. Ethnobiol. Ethnomed. 4 (2008) 13.
[8] Boi M. The Ethnocultural significance for the use of plants in Ancient Funerary Rituals and its possible implications with pollens found on the Shroud of Turin. Congreso Internacional sobre la Sábana Santa en España; Spain: Valencia. (2012) 1–20.
[9] U. Mayer-Chissick, et al., Wild edible plants in israel tradition versus cultivation. Medicinal and Aromatic Plants of the Middle-East, Springer,, 2014, pp. 9–26.
[10] E. Bagcı, et al., Essential oils of two varieties of *Gundelia tournefortii L.* (Asteraceae) from Turkey, Asian J. Chem. 22 (2010) 6239–6244.
[11] M. Asadi-Samani, et al., Gundelia: a systematic review of medicinal and molecular perspective, Pak. J. Biol. Sci. 16 (2013) 1238–1247.
[12] R.M. Darwish, et al., effect of ethnomedicinal plants used in folklore medicine in Jordan as antibiotic resistant inhibitors on Escherichia coli, BMC Complement Alter. Med. 28 (2010) 9.
[13] A. Mavi, et al., Inhibition of iron- fructose- phosphate- induced lipid peroxidation by ethanol extracts of 10 edible plants, J. Food Biochem. 35 (2011) 833–844.
[14] S. Oryan, et al., Anti-nociceptive and anti-inflammatory effects of aerial parts of *Gundelia tournefortii L.* on NMRI male mice. Persian, J. Shahr-e-Kord Univ. Med Sci. 12 (2011) 8–15.
[15] A. Jamshidzadeh, et al., Hepatoprotective activity of *Gundelia tourenfortii*, J. Ethnopharmacol. 3 (2005) 233–237.
[16] B. Matthäus, et al., Chemical evaluation of flower bud and oils of tumbleweed (*Gundelia tourneforti L.*) as a new potential nutrition sources, J. Food Biochem. 35 (2011) 1257–1266.
[17] M. Kieliszek, et al., Application of sodium selenite in the prevention and treatment of cancers, Cells 63 (2017) 9.
[18] S. Farkona, et al., Cancer immunotherapy: the beginning of the end of cancer? BMC Med. 14 (2016) 73.
[19] G.M. Cooper, in: (M.A.) Sunderland (Ed.), The Cell: A Molecular Approach, second ed., Sinauer Associates, 2000.
[20] T. Bender, et al., Where killers meet–permeabilization of the outer mitochondrial membrane during apoptosis, Cold Spring Harb. Perspect. Biol. 5 (2013), a011106.
[21] Y.-P. Zhu, et al., Primary hepatic angiosarcoma: a report of two cases and literature review, World J. Gastroenterol. 21 (2015) 6088.
[22] L.D. Shultz, B.L. Lyons, L.M. Burzenski, B. Gott, X. Chen, S. Chaleff, M. Kotb, S. D. Gillies, M. King, J. Mangada, D.L. Greiner, R. Handgretinger, Human lymphoid and myeloid cell development in NOD/LtSz-scid IL2R gamma null mice engrafted with mobilized human hemopoietic stem cells, J. Immunol. 174 (2005) 6477–6489.
[23] K. Fukuzawa, A. Tokumura, Glutathione peroxidase activity in tissues of vitamin E deficient mice, J. Nutr. Sci. Vitam. 22 (1976) 405–407.

[24] O. Krenkel, et al., Liver macrophages in tissue homeostasis and disease, Nat. Rev. Immunol. 17 (2017) 306–321.
[25] V. Hernandez-Gea, et al., Role of the microenvironment in the pathogenesis and treatment of hepatocellular carcinoma, Gastroenterology 144 (2013) 512–527.
[26] X.J. Hou, et al., Immune response involved in liver damage and the activation of hepatic progenitor cells during liver tumorigenesis, Cell Immunol. 326 (2018) 52–59.
[27] C.S. Melincovici, et al., Vascular endothelial growth factor (VEGF) - key factor in normal and pathological angiogenesis, Rom. J. Morphol. Embryol. 59 (2018) 455–467.
[28] Y. Zhang, et al., TGF-β family signaling in the control of cell proliferation and survival, Cold Spring Harb. Perspect. Biol. 9 (2017), a022145.
[29] G. Song, et al., TIMP1 is a prognostic marker for the progression and metastasis of colon cancer through FAK-PI3K/AKT and MAPK pathway, J. Exp. Clin. Cancer Res. 20 (2016) (13046-016).
[30] T. Aikawa, et al., Glypican-1 modulates the angiogenic and metastatic potential of human and mouse cancer cells, J. Clin. Investig. 118 (2008) 89–99.
[31] M. Capurro, et al., Glypican-3 as a serum marker for hepatocellular carcinoma, Cancer Res. 65 (2005) 372.
[32] M.M. Yeh, D.E. Bosch, S.S. Daoud, Role of hepatocyte nuclear factor 4-alpha in gastrointestinal and liver diseases, World J. Gastroenterol. 25 (2019) 4074–4091.
[33] A.J. Watt, W.D. Garrison, S.A. Duncan, HNF4: a central regulator of hepatocyte differentiation and function, Hepatology 37 (2003) 1249–1253.
[34] X. Zhan, A. Zhao, Transcription factor FOXA3 promotes the development of Hepatoblastoma via regulating HNF1A, AFP, and ZFHX3 expression, J. Clin. Lab Anal. 35 (2021), e23686.
[35] O. Alder, R. Cullum, S. Lee, A.C. Kan, W. Wei, Y. Yi, V.C. Garside, M. Bilenky, M. Griffith, A.S. Morrissy, G.A. Robertson, N. Thiessen, Y. Zhao, Q. Chen, D. Pan, S. J.M. Jones, M.A. Marra, P.A. Hoodless, Hippo signaling influences HNF4A and FOXA2 enhancer switching during hepatocyte differentiation, Cell Rep. 9 (2014) 261–271.
[36] X. Ding, Y. Yang, B. Han, C. Du, N. Xu, H. Huang, T. Cai, A. Zhang, Z.G. Han, W. Zhou, L. Chen, Transcriptomic characterization of hepatocellular carcinoma with CTNNB1 mutation, PLoS One 5 (2014), e95307.
[37] H. Okabe, S. Satoh, T. Kato, O. Kitahara, R. Yanagawa, Y. Yamaoka, T. Tsunoda, Y. Furukawa, Y. Nakamura, Genome-wide analysis of gene expression in human hepatocellular carcinomas using cDNA microarray: identification of genes involved in viral carcinogenesis and tumor progression, Cancer Res. 61 (2001) 2129–2137.
[38] T. Scholzen, J. Gerdes, The Ki-67 protein: from the known and the unknown, J. Cell Physiol. 182 (2000) 311–322.
[39] D.L. Wheeler, Y. Yarden, Receptor Tyrosine Kinases: Family and Subfamilies, Springer, New York, United States, 2015.
[40] N. Nishida, A. Goel, Genetic and epigenetic signatures in human hepatocellular carcinoma: a systematic review, Curr. Genom. 12 (2) (2011) 130–137.
[41] K.H. Vousden, et al., p53 and metabolism, Nat. Rev. Cancer 9 (2009) 691–700.
[42] V. Henderson, et al., Snail promotes cell migration through Pi3K/Akt-dependent rac1 activation as well as Pi3K/Akt-independent pathways during prostate cancer progression, Cell Adhes. Migr. 9 (2015) 255–264.
[43] I. Vivanco, et al., The phosphatidylinositol 3-Kinase AKT pathway in human cancer, Nat. Rev. Cancer 2 (2002) 489–501.
[44] G. Ferrín, M. Guerrero, V. Amado, M. Rodríguez-Perálvarez, M. De la Mata, Activation of mTOR signaling pathway in hepatocellular carcinoma, Int. J. Mol. Sci. 21 (4) (2020) 1266.
[45] C. Chang, et al., Reversal of multidrug resistance by two nordihydroguaiaretic acid derivatives, M4N and maltose-M3N, and their use in combination with doxorubicin or paclitaxel, Cancer Chemother. Pharmacol. 58 (2006) 640–653.
[46] F. Calderon, et al., Detection of intracellular phosphatidylserine in living cells, J. Neurochem. 104 (2008) 1271–1279.
[47] B. Halliwell, J.M.C. Gutteridge, Free Radicals in Biology and Medicine, Oxford UniversityPress, Oxford, London, UK, 1999.
[48] H. Lu, M.H. Stenzel, Multicellular tumor spheroids (MCTS) as a 3D in vitro evaluation tool of nanoparticles, Small 14 (2018), e1702858.
[49] R.B. Mokhtari, B. Qorri, M. Sambi, N. Baluch, S. Kumar, B. Das, M.R. Szewczuk, H. Yeger, H.M. Cheng, 3D multicellular stem-like human breast tumor spheroids enhance tumorigenicity of orthotopic xenografts in athymic nude rat model, Cancers 13 (2021) 2784.
[50] T. Ishiguro, H. Ohata, A. Sato, K. Yamawaki, T. Enomoto, K. Okamoto, Tumor derived spheroids: relevance to cancer stem cells and clinical applications, Cancer Sci. 108 (2017) 283–289.
[51] S. Abu- Lafi, et al., Anticancer activity and phytochemical composition of wild Gundelia tournefortii, Oncol. Lett. 17 (2019) 713–717.
[52] B. Özaltun, et al., Evaluation of antimicrobial activities and in vitro cytotoxic activities of gundelia tournefortii L. plant extracts, SDÜ Tıp Fakültesi Derg. 26 (2019) 436–442.
[53] P. Liu, et al., Cell-cycle-regulated activation of Akt kinase by phosphorylation at its carboxyl terminus, Nature 24 (2014) 541–545.
[54] J. Luo, et al., Targeting the PI3K-Akt pathway in human cancer: rationale and promise, Cancer Cell 4 (2003) 257–262.
[55] J. Ferlay, et al., Cancer incidence and mortality worldwide: sources, methods and major patterns in GLOBOCAN 2012, Int. J. Cancer 136 (2015) 359–386.
[56] L. Xerri, J. Adélaïde, C. Popovici, S. Garnier, A. Guille, L. Mescam-Mancini, et al., CDKN2A/B deletion and double-hit mutations of the MAPK pathway underlie the aggressive behavior of langerhans cell tumors, Am. J. Surg. Pathol. 42 (2018) 150–159.
[57] Y. Zhang, Y. Xiong, W.G. Yarbrough, ARF promotes MDM2 degradation and stabilizes p53: ARF-INK4a locus deletion impairs both the Rb and p53 tumor suppression pathways, Cell 92 (1998) 725–734.
[58] J.P. Luo, J. Wang, J.H. Huang, CDKN2A is a prognostic biomarker and correlated with immune infiltrates in hepatocellular carcinoma, Biosci. Rep. 39 (2021) (BSR20211103).
[59] Abdul M. Oseini, R.Roberts Lewis, PDGFRα: a new therapeutic target in the treatment of hepatocellular carcinoma? Expert Opin. Ther. Targets 13 (4) (2009) 443–454.
[60] J. Zheng, et al., Prediction of hepatocellular carcinoma recurrence beyond milan criteria after resection: validation of a clinical risk score in an international cohort, Ann. Surg. 266 (2017) 693–701.
[61] X.P. Chen, et al., Long-term outcome of resection of large hepatocellular carcinoma, Br. J. Surg. 93 (2006) 600–606.
[62] K. Boylan, R.D. Manion, H. Shah, K.M. Skubitz, A. Skubitz, Inhibition of ovarian cancer cell spheroid formation by synthetic peptides derived from nectin4, Int. J. Mol. Sci. 21 (2020) 4637.
[63] V. Laszlo, Z. Valko, J. Ozsvar, et al., The FAK inhibitor BI 853520 inhibits spheroid formation and orthotopic tumor growth in malignant pleural mesothelioma, J. Mol. Med. 97 (2019) 231–242.
[64] Y. Xu, X. Guo, G. Wang, C. Zhou, Vitamin C inhibits metastasis of peritoneal tumors by preventing spheroid formation in ID8 murine epithelial peritoneal cancer model, Front. Pharmacol. 12 (2022) 645.
[65] D. Melnik, J. Sahana, T.J. Corydon, S. Kopp, M.Z. Nassef, M. Wehland, M. Infanger, D. Grimm, M. Krüger, Dexamethasone inhibits spheroid formation of thyroid cancer cells exposed to simulated microgravity, Cells 9 (2021) 367.